IEEE Access
Multidisciplinary | Rapid Review | Open Access Journal

Received June 15, 2019, accepted June 20, 2019, date of publication June 24, 2019, date of current version July 11, 2019.

Digital Object Identifier 10.1109/ACCESS.2019.2924557

Cognitive Competence Improvement for Autonomous Vehicles: A Lane Change Identification Model for Distant Preceding Vehicles

CHANG WANG[1,2], QINYU SUN[1,2], ZHEN LI[1,2,3], HONGJIA ZHANG[1,2], AND KAILI RUAN[1]

[1]School of Automobile, Chang'an University, Xi'an 710064, China
[2]Key Laboratory of Automotive Transportation Safety Technology, Xi'an 710064, China
[3]School of Kinesiology, University of Minnesota, Minneapolis, MN 55455, USA

Corresponding authors: Qinyu Sun (sunqinyu@chd.edu.cn) and Zhen Li (lzhen093@gmail.com)

This work was supported in part by the National Key R&D Program of China under Grant 2018YFB1600501, in part by the Changjiang Scholars and Innovative Research Team in University under Grant IRT_17R95, and in part by the National Natural Science Foundation of China under Grant 51775053.

ABSTRACT The motion status recognition of the preceding vehicle in a long-distance region is a requirement for autonomous vehicles to make appropriate decisions and increase their comprehension of the environment. At present, the lane change behavior of the leading vehicle at a short distance is detected using stereo cameras and LiDAR. However, the short detection distance (about 100 m) does not meet the requirements of high-speed driving of autonomous vehicles on expressways; this is a fundamental problem limiting the development of autonomous vehicles exhibiting human-like behavior. In this paper, a comprehensive model consisting of a back-propagation (BP) neural network model optimized by a particle swarm optimization (PSO) algorithm, and a continuous identification model is developed based on the results of naturalistic on-road experiments using millimeter-wave radar data. By considering different time-to-lane crossings (TLCs), the PSO-BP neural network model is trained using real vehicle lane change data and implemented when the TLC of the leading vehicle is longer than 1.0 s. In contrast, when the TLC is less than 1 s, the continuous recognition model of the TLC is used. By comparison with the BP neural network model, the recognition accuracy rate of the proposed model is increased from 80% to 87% after the PSO optimization for a time window of 1.0 s; these results meet the recognition requirements of the autonomous driving systems for distant targets. The findings of this paper improve the cognitive competence and safety of autonomous driving systems.

INDEX TERMS Autonomous driving perception, cognitive competence, lane change behavior, BP neural network.

I. INTRODUCTION

Autonomous driving systems have developed progressively and have been demonstrated by vehicle safety organizations to improve the safety of driving and reduce traffic collisions [1]–[3]. Autonomous driving systems anticipate potential accidents and promptly deliver the information to the decision-making system based on a precise perception of the traffic environment, including the movements of surrounding vehicles and pedestrians and the presence of traffic signs [4], [5]. The main cause of accidents of autonomous vehicles during road tests is that the autonomous systems do not identify the motion status of surrounding vehicles accurately [6]–[8]. At present, the lane change detection of preceding vehicles within a short distance range (about 100 m) is accurately identified using stereo cameras and LIDAR [9]–[11]. However, due to the limitation of the sensor detection distance, the motion status of the leading vehicle cannot be precisely detected, resulting in a potential safety hazard for high-speed driving of autonomous vehicles on expressways [12]–[14]. Therefore, the identification of the motion status of potential conflicting targets in the distant

The associate editor coordinating the review of this manuscript and approving it for publication was Shaohua Wan.

range is crucial for improving the cognitive competence of autonomous vehicle systems with regard to the traffic environment and developing autonomous vehicle systems with human-like behavior.

In actual driving, the abrupt lane change behavior of a leading vehicle has a significant impact on the subject vehicle and the possibility of a rear-end collision is greatly increased when the subject vehicle is compelled to change lanes as well [15]–[17]. In an adaptive cruise control (ACC) system, the cruising speed may suddenly be reduced when an unexpected vehicle changes into the target lane and the large change in velocity may cause driver discomfort [18]. However, if the lane change behavior of the leading vehicles could be identified in advance, the ACC system can adjust the velocity of the subject vehicle more smoothly. Similarly, a lane change warning system may detect in time the potential danger of a leading vehicle that intends to change into the target lane from another lane [19]. The system can then deliver an alarm to the decision-making system if the lane change behavior of the leading vehicle is recognized in advance. In an autonomous vehicle, the lane change detection of the preceding vehicle affects the subsequent decisions of the system. In brief, lane change identification is essential for exploiting intelligent algorithms that provide responses that are similar to those of a person. Accurate and prompt recognition provides the basis for other auxiliary decision systems. Hence, the establishment of the identification model is regarded as the key to perception technologies [20]. The current lack of this technology limits the cognitive competence of autonomous systems and impacts the safety of autonomous vehicles.

Over the years, researchers have developed methods to improve the performance of identifying the vehicle lane change status. At present, traditional machine learning methods, such as support vector machines (SVM), hidden Markov models (HMM), and artificial neural networks (ANN) have been widely employed to establish lane change identification models. Zheng *et al.* [21] established an ANN model for discerning left-lane changes and right-lane changes by considering the distance, speed, and acceleration of different. Prevost *et al.* [22] defined the kinestate and predicted the route of mobile vehicles using an extended Kalman filter. Hermes *et al.* [23] proposed a prediction model for the motion status that combined trajectory classifications and particle filters; the trajectories were classified using a radial basis function classifier and a particle filter was used for trajectory tracking. This approach was validated by forecasting the movement of a subject vehicle and ambient vehicles within seconds. Dou *et al.* [24] suggested that combining an SVM and a neural network by using weight allocations could improve the recognition rate for lane changes; vehicle data were extracted, including horizontal and vertical coordinates, speed, and type, from the next-generation simulation (NGSIM) database. Haijing *et al.* [25] developed an identification model for lane change intention that integrated a hybrid Gaussian HMM with a SVM and used the standard deviation of the horizontal angle of the driver's head, the number of times the driver gazed at the rear-view mirror, the average scanning range, and the steering wheel angle entropy as input parameters. Semantic segmentation and target detection based on deep learning techniques have been used to detect the motion state of the target using data derived from stereo cameras and LIDAR [26]–[29]. However, the detection range of a stereo camera does not exceed 100 m and the range of the LIDAR is only about 120 m. This detection distance ensures the safety of autonomous driving at low-speed but for high-speed driving on expressways, this short detection results in extensive risks to the autonomous vehicle and other drivers. Therefore, the detection and recognition of distant targets currently depend on the use of millimeter-wave radar (the detection distance is about 200 m).

The determination of the time window is a key factor in the development of detection models of the vehicle lane change status [30]. The optimal time window results in a higher detection rate and greater efficiency of the back-propagation neural network (BPNN) model. The longer the time window, the larger the amount of gathered information is and the higher the recognition rate is, but the model cannot immediately determine the motion status of the vehicle. In contrast, a rapid decision can be obtained using a shorter time window but the recognition rate is lower. The length of the time window determines the amount of information that is obtained by the model. Scholars have used different time windows to determine the lane change status. Doshi and Trivedi [31] established a recognition model of lane change intentions based on the driver's head posture and eye movement trajectory; the results demonstrated that the model had the best recognition performance for a time window of 3 s. Lethaus and Rataj [32] determined a time window of 10 s by exploiting the driver's eye movement characteristics to analyze the lane change behavior. Jin *et al.* [33] divided the time windows of the lane change identification model into 5 s, 3 s, and 2 s, depending on different driving styles. The driving intention identification model proposed by Zong *et al.* [34] used a time window of 0.08 s to recognize the driver's short-term operation. The results of these studies indicate that the time window can vary from 0.08 s to 10 s, representing a rather large range. Therefore, the appropriate time window should be considered in terms of accuracy and real-time performance and based on the actual lane change behavior and the specific situation.

At present, research has mainly concentrated on the identification of the lane change status of the subject vehicle and few studies were conducted on the recognition of the lane change status of leading vehicles. When the leading vehicle was the research focus, most of the commonly used parameters for the prediction of driver lane change behavior, such as eye movements and head movements could not be obtained by the subject vehicle. Only the lateral and longitudinal parameters of the leading vehicle can be collected using millimeter-wave radar. In view of this disadvantage, we identified the relative kinematic parameters of the subject

and leading vehicles by using the results of the naturalistic on-road experiment. We propose a comprehensive recognition model based on a BPNN optimized by a particle swarm optimization (PSO) algorithm and a continuous identification model of time-to-lane crossing (TLC). The remainder of this paper is organized as follows. The related studies on ANNs and PSO algorithm are discussed in Section II. The proposed identification model for the lane change status based on a BPNN and PSO algorithm for optimization is described in Section III. The training data for the proposed PSO-BPNN model are presented in Section IV. The simulation results and analysis are described in Section V. The conclusions are presented in Section VI.

II. RELATED STUDIES

The essence of the identification model is to extract the characteristic differences among disparate data, thereby establishing a mapping relationship between the input data and the target identifier and minimizing the error [35]. Currently used recognition models may be roughly divided into production models, discriminative models, and learning models. Production models calculate the internal potential probability of the data and classify it by means of probability maximization [36], [37]. These models include the HMM, the naive Bayes classifier, and the mixed Gaussian model. HMMs have been widely used for the identification of driving intention and behavior [38]. However, the HMM requires that the events be independent of each other and the HMM is a linear model, which is not suitable for complex identification problems. Discriminative models recognize the targets by analyzing the regional characteristics inside the feature space. These types of models include the SVM, conditional random fields, and similar models. However, the greatest disadvantage of these models is the inability to support a large number of training samples [39]. Learning models are patterned after the learning behavior of biological organisms and various neural network models are representatives of this type of model. Particularly, ANN models based on the structure of the brain have been used to solve complex recognition problems and these model have a good tolerance for erroneous data [40]. At present, many identification models based on ANNs have been used to recognize the motion status of vehicles. Zhou *et al.* [41] used a miniature car and developed a following model based on a recurrent neural network for the accurate determination of traffic fluctuations. Liu and Jing [42] constructed a decision-making model based on a BPNN for vehicles driving on an expressway to detect the lane-changing behavior. A quick response controller for steering control based on an ANN was implemented by Aalizadeh and Asnafi [43] for vehicle handling in uncertain road conditions.

In spite of the significant development of ANN models, it was found that complex nonlinear optimization problems cannot be efficiently solved by the available neural network models. In particular, some problems persist, such as the difficulty of determining the initial connection weight thresholds and the slow convergence of BPNNs [44]. The gradient descent method used in BPNNs is highly sensitive to the initial connection weight and the set threshold [45]; therefore, the selection of different initial values may lead to different training results and there exists sparse theoretical guidance for determining the appropriate weight and threshold. To address these problems, numerous optimization algorithms have been employed and the optimized models with the optimal parameters were used to improve the mapping capability of BPNNs [46]. Kapanova *et al.* [47] proposed a novel automated method based on a genetic algorithm (GA) to search for BPNN architectures, which included the number of neurons, the number of hidden layers, and the types of synaptic connections. Taghavifar *et al.* [48] used a GA as an optimization tool to improve the reorganization ability of a BPNN. Zhu *et al.* [49] employed the PSO algorithm to optimize the initial weights and thresholds of the BPNN. The PSO algorithm has been used in different identification models for optimizing disparate parameters of neural networks; the selection of the optimization parameters should depend on the specific conditions. For tracking the applied operators and connections of layers of an ANN model, a hybrid model based on a BPNN model and the PSO algorithm were proposed by Hao *et al.* [50] to forecast the number of end-of-life vehicles. A parallel design and application method for implementation of the PSO-BPNN was proposed by Liu *et al.* [51]. However, given the discrepancy of the input data, a model for the identification of the behavior of surrounding vehicles still faces significant challenges.

III. MODEL FRAMEWORK

A. FRAMEWORK DESIGN

To achieve the rapid and accurate identification of the motion status of a distant leading vehicle, in this study, a comprehensive recognition model was proposed to ensure that all lane changes of the leading vehicles were detected. Considering the difference in the time-to-lane crossing (TLC), the identification model can be divided into two parts, namely, the PSO-BPNN model and the continuous identification model of the TLC. The lateral distance, lateral velocity, and longitudinal velocity of the leading vehicle were deduced from naturalistic driving data and this information was used to train the reorganization model based on the BPNN. Due to the slow rate of convergence of the BPNN and the possibility of falling into a local minimum, in this study, we use the PSO algorithm to optimize the initial connection weights and thresholds of the BPNN. In the following section, we present some brief explanations of the PSO-BPNN model. The continuous identification model of the TLC replaced the PSO-BPNN when the TLC of the leading vehicle was shorter than the time window. The TLC is defined as the time required for the leading vehicle to cross the lane from the start position. The TLC is a key indicator of safe driving. The TLC is defined in (1). By continuously subdividing the TLC interval, the lane change probability within each interval can be calculated.

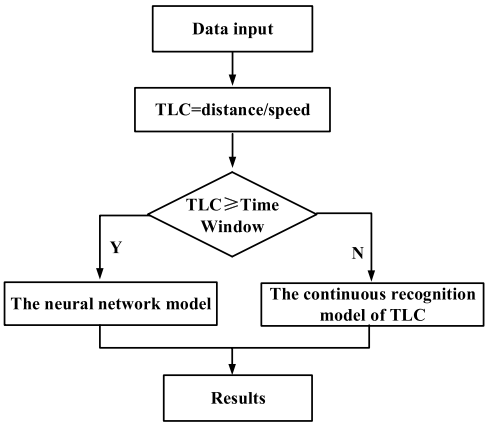

FIGURE 1. The flowchart of the comprehensive identification model.

The flowchart of the comprehensive identification model is shown in Fig. 1. The PSO-BPNN model was implemented when the TLC of the leading vehicle was longer than 1.0 s, whereas the continuous recognition model of the TLC was used when the TLC was less than 1.0 s.

$$TLC = dis/speed \tag{1}$$

where *TLC* is the lane crossing time, *dis* is the lateral distance between the leading vehicle and the lane, and *speed* is the lateral velocity of the leading vehicle.

B. BPNN DESIGN

The learning process of a BPNN is achieved by the forward transmission of data and the reverse transmission of the error. When the level of error exceeds the expected range, the BP of the error is implemented and the network weights and thresholds are calibrated layer by layer according to the error value [52]. The training process commonly comprises the following seven steps: network initialization, output value calculation of the hidden layers, output value calculation of the output layers, error calculation, updating of weights, updating of thresholds, and termination judgment. The processes are described below.

$$e_k = Y_k - O_k k = 1, 2, \ldots, m \tag{2}$$

$$w_{ij} = w_{ij} + \eta H_j \left(1 - H_j\right) x\left(i\right) \sum_{k=1}^{m} w_{jk} e_k \tag{3}$$

$$w_{jk} = w_{jk} + \eta H_j e_k \tag{4}$$

$$a_j = a_i + \eta H_j \left(1 - H_j\right) \sum_{k=1}^{m} w_{jk} e_k \tag{5}$$

$$b_k = b_k + e_k \tag{6}$$

where e_k is the forecast error, O_k is the predicted output value, Y_k is the desired output value, w_{ij} and w_{jk} are the weight values, a_j and a_i are the hidden layer thresholds, H_j is the hidden layer output value, $x(i)$ is the output variable, b is the output layer threshold, and η is the learning rate.

Parameter training is the primary kernel for the establishment of the BPNN model [53]–[55]. The determination of the learning rate and the learning method directly affect the performance of the BPNN model. The larger the confirmed learning rate, the greater the modification value of the weights would possess. However, the weights may fluctuate and become unstable when the output value approaches the target value if the learning rate was too high. In this study, a variable learning rate was used. A large value for the learning rate was used in the initial stage to ensure the rapid convergence of the neural network. The value of the learning rate decreased as the output data gradually approached the target value. The variable learning rate is defined in (7).

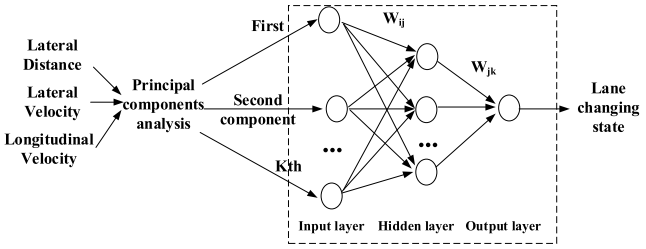

FIGURE 2. BPNN structural diagram.

$$\eta(n) = \eta_{max} - n(\eta_{max} - \eta_{min})/n_{max} \tag{7}$$

where η_{max} is the maximum learning rate, η_{min} is the minimum learning rate, and n is the number of iterations.

The gradient correction method modifies the weights and the thresholds in the direction of the negative gradient of the prediction error. However, due to the lack of accumulation of previous experience, the learning speed of this method was relatively slow. Therefore, an additional momentum method was used to solve the problem of the slow convergence of the gradient correction method; the computational process is defined as:

$$w\left(n\right) = w\left(n-1\right) + \alpha\left(w\left(n\right) - w\left(n-1\right)\right) + \beta\left(w\left(n-1\right) - w\left(n-2\right)\right) \tag{8}$$

where *w(n)*, *w(n-1)*, and *w(n-2)* are the weights of *n* iterations, *n-1* iterations, and *n-2* iterations, respectively; α and β are the momentum learning rates.

A BPNN provides an intuitive and effective approach to determine the complex nonlinear mapping relationships between the lane change status of the leading vehicles and the kinematic parameters that define the driving process. After normalization of the input parameters and principal components analysis, the proposed model can detect the lane change status of leading vehicles according to the data characteristics within a time window. The structure of the BPNN is shown in Fig. 2. The longitudinal velocity, lateral velocity, and lateral distance of the leading vehicle were used as input variables in this work. The optimal input combination was determined by evaluating the identification accuracy of the neural network model under different input combinations. The different input combinations are shown in Table 1.

C. PSO-BPNN MODEL DESIGN

By searching for the optimal connection weights and thresholds, the BP algorithm continuously minimizes the output error of the training model. Since the gradient descent method

TABLE 1. Combinations of input parameters.

Number	Combinations of input parameters
1	Lateral Distance (LD)
2	Lateral Velocity (LV)
3	Lateral Distance (LD), Lateral Velocity (LV)
4	Lateral Distance (LD), Longitudinal Velocity (ZV)
5	Lateral Velocity (LV), Longitudinal Velocity (ZV)
6	Lateral Distance (LD), Lateral Velocity (LV), Longitudinal Velocity (ZV)

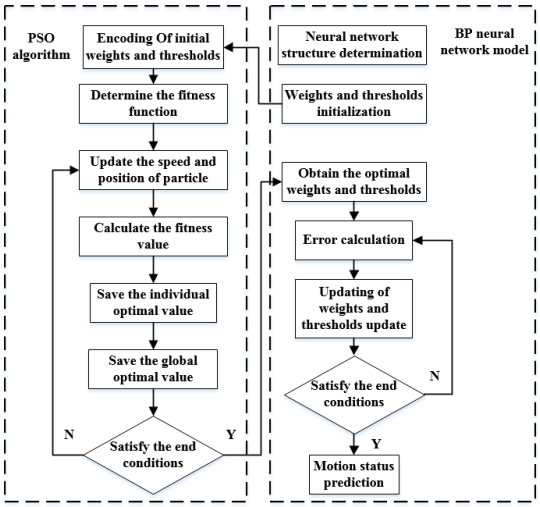

FIGURE 3. The flowchart of BPNN optimization based on the PSO algorithm.

is extremely sensitive to the initial values of the connection weights and thresholds, different initial values will lead to different training results [56]. However, there is no relevant theoretical guidance for choosing the initial connection weights and threshold. In addition, the BPNN often falls into a local extremum and cannot find a globally optimal solution, which weakens the generalization ability of the BPNN model. In order to address these disadvantages of the BPNN, the PSO algorithm was used to optimize the proposed model [57]. The PSO algorithm is a meta-heuristic algorithm based on swarm intelligence. The aim of the PSO algorithm is to find the best solution by simulating the particle movements in the search space [58]. In this study, the PSO algorithm was employed to optimize the initial weights and thresholds of the BPNN model. We determined the sum of weights and thresholds in the BPNN as the vector dimension of particles; each particle position corresponded to a set of feasible solutions of the weights and thresholds. The variation of the particle positions indicated the continuous updating process of the weights and thresholds. By calculating the fitness value, the particle position with the smallest fitness value was confirmed as the optimal initial weights and thresholds for the BPNN. The specific steps are described as follows and the basic flow of the BPNN optimization based on the PSO algorithm is shown in Fig. 3.

Step 1: PSO-BPNN initialization. The initialization included setting the parameters of the BPNN and PSO algorithm (i.e., the number of input layer nodes, hidden layer nodes, and particles; the initial position and speed of the particles and the vector dimension of particles). Then the connection weights and thresholds in the BPNN were encoded according to the vector dimension of the particles and the initial position and velocity of the particles. The vector dimension of the particles was obtained using (9).

$$D = m * n + n * p + q + s \tag{9}$$

where D is the vector dimension of the particles, m is the number of the input layer nodes, n is the number of the hidden layer nodes, p is the number of the output layer nodes, $m*n$ is the number of the connection weights between the input layer and the hidden layer, $n*p$ is the number of the connection weights between the hidden layer and the output layer, q is the number of the hidden layer thresholds, s is the number of the output layer thresholds.

Step 2: Fitness function selection and fitness value calculation. The absolute error between the expected output and predicted output of the BPNN was calculated; the fitness function is defined in (10); each individual particle's fitness value was calculated.

$$f = \frac{1}{n}\sum_{j=1}^{n}(\tilde{y}_j - y_j)^2 \tag{10}$$

where n is the number of samples in the training set, $\tilde{y}_j$ is the output of the BPNN, and y_j is the expected output.

Step 3: Updating of the optimal value. For each particle, if the current position possessed a smaller fitness value than the previous individual optimal value, then the current position was confirmed as the individual optimal value; if the current position possessed a smaller fitness value than the previous global optimal value, then the current position was confirmed as the global optimal value.

Subsequently, the speed and position of the particles were updated. The PSO algorithm simulates the foraging behavior of birds in flight. By using local and global optimizations, the particles are directed toward the optimal solution [59]. The particles dynamically update their speeds and positions according to their flying experience in the solution space and the flying state of the whole population. The updated positions and speeds during the flying process are defined in (11) and (12), respectively. The inertia weights were also updated for generating new populations. In order to avoid that the PSO algorithm falls into a local optimum, a linearly decreasing weight method was employed to update the inertia weight, as defined in (13).

$$v_{ij}^{k+1} = wv_{ij}^{k} + c_1 r_1\left(p_{ij} - x_{ij}^{k}\right) + c_2 r_2\left(p_{gj} - x_{ij}^{k}\right) \tag{11}$$

$$x_{ij}^{k+1} = x_{ij}^{k} + v_{ij}^{k+1} \tag{12}$$

$$w = w_{max} - k(w_{max} - w_{min})/k_{max} \tag{13}$$

where x is the position, v is the velocity, w is the inertia weight, c_1 and c_2 are the acceleration coefficients, r_1 and r_2

are random numbers between zero and one, p_{ij} is the optimal position (i.e., the optimal fitness value) of the individual particle until the current population, p_{gj} is the optimal position (i.e., the optimal fitness value) of the global particles until the current population, w_{max} is the maximum inertia weight, w_{min} is the minimum inertia weight, k_{max} is the maximum number of iterations.

Finally, the predetermined threshold of the optimal fitness value was used to determine whether to end the algorithm loop. The predetermined threshold of the optimal fitness value indicates that the current connection weights and thresholds can improve the convergence speed and global optimization ability of BPNN. If the fitness values in the current population reached the predetermined range, the positions of the global particles were determined as the initial weights and thresholds of the BPNN model. In contrast, the positions of the particles were updated and the fitness values were recalculated. After the determination of the initial weights and thresholds, the BPNN was used to train the model using the conventional steps. In general, the selection of the predetermined threshold value is directly related to the accuracy of the recognition model results. The PSO optimization algorithm can be summarized in Algorithm 1.

Algorithm 1 BPNN Optimization Based on the PSO Algorithm

Data: the number of the input layer nodes m, the number of the hidden layer nodes n, the number of the output layer nodes p, the number of the hidden layer thresholds q, the number of the output layer thresholds s, the acceleration coefficients c_1 and c_2

Result: the initial weights and thresholds of the BPNN model

begin

Input and initialization

While $k < kmax$

for $i = 1 : n$

$$v_{ij}^{k+1} = wv_{ij}^{k} + c_1 r_1 \left(p_{ij} - x_{ij}^{k}\right) + c_2 r_2 \left(p_{gj} - x_{ij}^{k}\right)$$

$$x_{ij}^{k+1} = x_{ij}^{k} + v_{ij}^{k+1}$$

$$w = w_{max} - k(w_{max} - w_{min})/k_{max}$$

end

for $j = 1 : n$

if $f(x_i) > f(p_i)$

$p_i = x_i$

if $f(p_i) > f(p_g)$

$p_g = p_i$

end

end

IV. TRAINING DATA

Training sample establishment is a preliminary work for the PSO-BPNN model training. In this work, we employed naturalistic driving data to extract characteristic parameters of lane change behaviors of distant preceding vehicles. By using a discrete Kalman filter, the interference in the original data were filtered out; and dimensionality reduction was employed to convert the data in the high-dimensional space into data values the low-dimensional space. The establishment of training samples and the pre-processing of input data provided support for improving the efficiency of the recognition model training.

FIGURE 4. Components of the data collection platform.

A. DATA DESCRIPTION

A total of 41 experienced drivers (i.e., 36 male, 5 female) were recruited to participate in the naturalistic driving test. During the naturalistic driving experiments, all participants were only informed of the initial points and destinations; no other instructions were given. The participants could navigate the host vehicle as they saw fit under the premise of obeying the rules and ensuring driving safety. The kinematic parameters of the leading vehicle were obtained by using the actual vehicle test data while driving on a freeway. To achieve our research objective to use data from an on-road test, we developed an integrated data gathering platform incorporated in a real vehicle. The platform comprised the following instruments and sensors: a millimeter-wave radar, GPS system, video monitoring system, vehicle gyro, CAN bus, and advanced warning system (AWS), among other instruments. The system components are shown in Fig. 4. During the naturalistic driving test, each participant was required to follow his or her normal habit of navigating. The lane change process of the leading vehicle was recorded via the video monitoring system and the distances between the lanes and subject vehicle were obtained by the AWS in our test vehicle. The kinestate parameters of the preceding vehicle, such as the lateral position in the lane, the relative velocity, and the relative distance were synchronously obtained by the sensors installed in our test vehicle. The collected real-time data provided the basis for establishing the leading vehicle lane change identification model and confirming the appropriate time window. In order to obtain as many lane change samples of the leading vehicles as possible, a closed two-way, 4-lane

FIGURE 5. The initial moment of the lane change behavior of the leading vehicle.

FIGURE 6. The termination moment of the lane change behavior of the leading vehicle.

TABLE 2. The sectional data obtained by the sensors.

Time (s)	Distance to left lane(cm)	Distance to right lane(cm)	Speed (km/h)	Relative angle (°)	Relative distance (m)	Relative velocity (m/s)
0.05	-45	135	81.40	17.1	13.1	4.55
0.10	-45	135	81.39	16.9	13.2	4.53
0.15	-45	135	81.33	15.9	14.0	4.46
0.20	-45	135	81.23	15.7	14.3	4.45
0.25	-45	135	81.06	14.8	14.8	4.44
0.30	-45	135	81.01	14.9	15.1	4.43
0.35	-45	140	81.03	15.1	15.3	4.42
0.40	-40	140	80.78	14.5	16.1	4.41
0.45	-40	140	80.66	13.8	16.6	4.40
0.50	-40	140	80.69	13.2	16.8	4.40
0.55	-40	140	80.74	13.0	17.1	4.38
0.60	-40	145	80.58	11.8	17.7	4.36
0.65	-40	145	80.48	11.4	17.8	4.33

freeway was selected for the driving experiments. On account of the heavy traffic and the limited number of lanes, more lane change behaviors were recorded than in experiments conducted on a 6-lane freeway.

B. DATA AND KALMAN FILTERING

Using the video monitoring system and the data from the AWS, the initial and termination moments of the lane change behavior of the distant leading vehicles were determined (Figs. 5 and 6). Simultaneously, the kinestate parameters deduced from the sensors were captured; the sectional data are shown in Table 2. The data include time, distance between the subject vehicle and the left lane, distance between the subject vehicle and the right lane, velocity of the subject vehicle, relative angle between the subject vehicle and the leading vehicle, relative distance between the subject vehicle

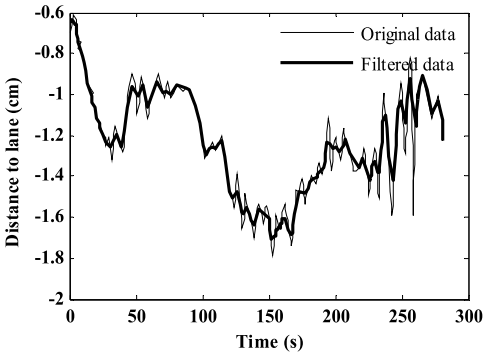

FIGURE 7. Comparison of original and filtered data of the distance to the lane.

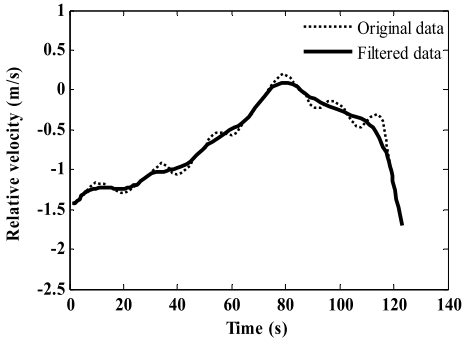

FIGURE 8. Comparison of original and filtered data of relative velocity.

and the leading vehicle, and the relative velocity between the subject vehicle and the leading vehicle. The actual data collected by the millimeter-wave radar was frequently mixed with random noise because of the random disturbances that occurred during the measurement of the motion parameters of the leading vehicles. Therefore, the required data must be isolated from the original data. Given this problem, we could not precisely determine the headway, speed, and other data for the leading vehicles. Hence, an estimation of the data according to the measured signals was used as an appropriate approach. Kalman filters incorporate the concept of state space in stochastic estimation theory and signal processing is regarded as a linear state influenced by white noise [60], [61]. In a statistical sense, the estimated value of the Kalman filtering is the probable value that is close to the real value. In the present study, a discrete Kalman filter [62] was used to filter the discrete data collected by the sensors. The results are shown in Figs. 7 and 8. As shown in the graph, the filtered data was smooth and the trend of the original data was preserved completely. Consequently, the Kalman filter was a suitable solution to the data perturbation problem.

C. REPRESENTATION PARAMETER DEDUCTION

The road curvature was calculated by the yaw rate and speed of the test vehicle, as defined in (14).

$$C = \frac{w_r}{v} = \frac{1}{R} \tag{14}$$

where C is the road curvature, w_r is the yaw rate,v is the test vehicle speed, and R is the radius of the road curvature.

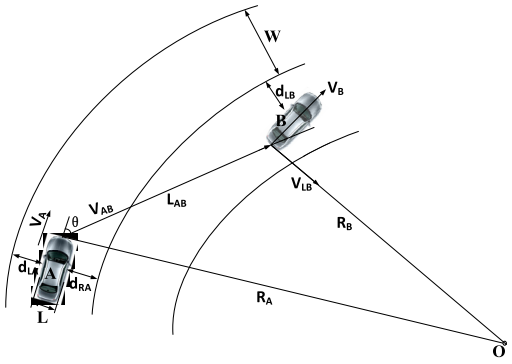

FIGURE 9. Characterization parameters of the curve.

In Fig. 9, A is the subject vehicle, B is the leading vehicle, R_A is the radius of the road curvature of the host lane, R_B is the radius of the road curvature of the adjacent lane, d_{RA} is the distance between the subject vehicle and the right lane, d_{LA} is the distance between the subject vehicle and the left lane, θ is the relative angle between the subject vehicle and the leading vehicle, L_{AB} is the relative distance between the subject vehicle and the leading-vehicle, V_{AB} is the relative velocity between the subject vehicle and the leading vehicle, L is the subject vehicle width, V_A is the subject vehicle velocity, V_B is the longitudinal velocity of the leading vehicle, V_{LB} is the lateral velocity of the leading vehicle, d_{LB} is the distance from the leading vehicle to the left lane, and W is the width of the lane. The relationship between R_A and R_B was obtained by analyzing the geometric relationships in Fig. 9. The road curvature of the test road ranged from 600 m to 1000 m and the width of the lane was 3.75 m.

$$R_B^2 = R_A^2 + L_{AB}^2 - 2R_A \times L_{AB} \times cos\,(90 - \theta) \tag{15}$$

The distance from the subject vehicle to the left lane is:

$$d_{LB} = R_A - R_B - d_{RA} - \frac{L}{2} \tag{16}$$

The formula for calculating the road radius is:

$$R_A = \frac{V_A}{w_r} \tag{17}$$

The distance from the subject vehicle to the left lane was deduced from (15), (16), and (17):

$$d_{LB} = \frac{V_A}{w_r} - \sqrt{\left(\frac{V_A}{w_r}\right)^2 + L_{AB}^2 - \frac{2V_A}{w_r} \times L_{AB} \times cos\,(90 - \theta)} - d_{RA} - \frac{L}{2} \tag{18}$$

The lateral distance fitting formula was established by selecting the lateral distance of the continuous time point. Then, the formula for the lateral velocity was deduced by using the derivative of the fitting formula.

$$V_{LB} = d_{LB}^{'} \tag{19}$$

The longitudinal velocity was calculated by using the relative velocity, relative angle, and subject vehicle velocity.

$$V_B = V_{AB} \times \cos\theta - V_A \tag{20}$$

As deduced from Fig. 9:

$$\alpha = 90 - \beta = 90 - (90 - \theta + \delta) = \theta - \delta \tag{21}$$

$$R_B^2 = R_A^2 + L_{AB}^2 - 2R_A \times L_{AB} \times cos\,(90 - \theta) \tag{22}$$

$$L_{AB}^2 = R_A^2 + R_B^2 - 2R_A \times R_B \times cos\delta \tag{23}$$

Then, the longitudinal velocity was refined as:

$$V_B = V_{AB} \times cos(\theta - \arccos \times \left(\frac{\frac{V_A}{w_r} - L_{AB} \times cos(90 - \theta)}{\sqrt{R_A^2 + L_{AB}^2 - \frac{2V_A}{w_r} \times L_{AB} \times cos(90 - \theta)}}\right)) - V_A \tag{24}$$

D. DIMENSIONALITY REDUCTION

The main purpose of dimensionality reduction is to convert the data in the high-dimensional space into data values the low-dimensional space [63], [64]. In general, the motion parameters of the leading vehicle are directly transformed into vectors, which serve as the model input. This process might result in data redundancy. Some variable values that are independent of the identified vehicle motion state are included in the model, which wastes processing resources and might affect the training model. Therefore, the training sample dimension must be minimized to improve training efficiency without losing important data. In contrast, the scope of the longitudinal velocity, lateral velocity, and lateral distance of the leading vehicle showed significant discrepancies. The longitudinal velocity varied from 20 to 120 km/h, the lateral velocity varied from 0 to 4 m/s, and the lateral distance varied from −7 to 3.5 cm. To a certain degree, the wide range of longitudinal velocity might conceal other data during the modeling process if the raw data were directly utilized as inputs. In order to minimize the problems caused by differences in dimension and magnitude, we normalized the original data. The normalization process is shown in (25).

$$y = (y_{max} - y_{min})\frac{x - x_{min}}{x_{max} + x_{min}} + y_{min} \tag{25}$$

where x_{max} and x_{min} are the maximum and minimum values of the data, respectively, y_{max} and y_{min} are the mapping ranges, which we set to $[-1, 1]$. The results are shown in Table 3.

Principal components analysis is a multivariate statistical method that uses dimensionality reduction to transform multiple indicators into fewer indicators. The method ensures that the remaining few indicators adequately contain the key information of the original variables. The principal components analysis is commonly used to simplify problems. In this study, the longitudinal velocity, lateral velocity, and lateral distance of the leading vehicle were used as variables in the principal component analysis. The contribution rate and cumulative contribution rate of each principal component are shown in Fig. 10. The cumulative contribution of the first four

TABLE 3. Normalization results.

Lateral velocity	Normalized LV data	Lateral distance	Normalized LD data
-0.055	-0.3750	-1.978	0.9758
-0.047	-0.0417	-1.971	1.0000
-0.035	0.4583	-1.997	0.9102
-0.030	0.6667	-2.043	0.7513
-0.026	0.8333	-2.114	0.5060
-0.023	0.9583	-2.159	0.3506
-0.022	1.0000	-2.205	0.1917
-0.022	1.0000	-2.232	0.0984
-0.024	0.9167	-2.225	0.1226
-0.0279	0.7542	-2.200	0.2090

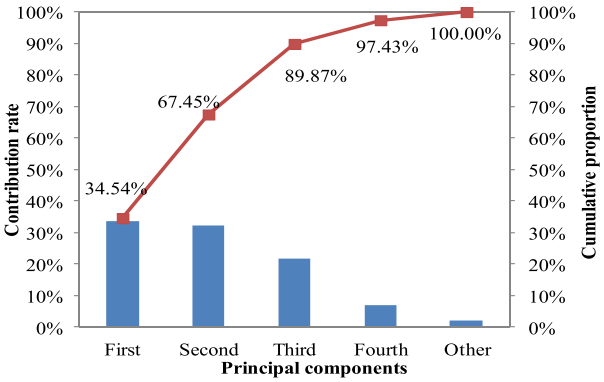

FIGURE 10. Cumulative contribution rate of the principal components.

principal components was 97.43%. Therefore, the parameters were expressed by the first four principal components.

V. RESULTS AND ANALYSIS

A. HIDDEN LAYER NODES OPTIMIZATION

The number of hidden layer nodes directly affects the performance of the BPNN; however, at present, there exists little theoretical guidance for the determination of the hidden layer nodes of the BPNN. When the number of hidden layer nodes is relatively small, the learning speed of the BPNN is fast but the learning ability for complex problems is not strong due to the simple structure of the model. In contrast, when the number of hidden layer nodes is relatively high, the learning ability is strong but the learning speed is slow due to the complex structure of the model. Sometimes, the learning ability decreases suddenly due to over-fitting. In order to balance the learning speed and the learning ability of the BPNN and to avoid over-fitting, it is necessary to optimize the number of hidden layer nodes.

An instance analysis was accomplished for determining the appropriate number of hidden layer nodes. The identification accuracy rate of the BPNN model for different numbers of hidden layer nodes was calculated using a time window of 1.0 s and the lateral distance and lateral velocity as the input parameters of the preceding vehicles. The number of input nodes was determined as 4 according to the results of the normalization and principal components analysis of the lateral distance data and lateral velocity data from the naturalistic driving test. The output of the BPNN model was the motion

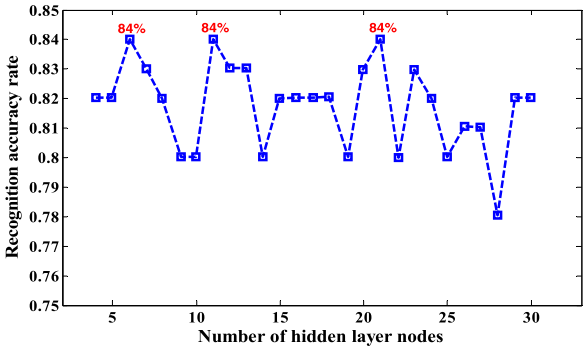

FIGURE 11. The identification accuracy rate of the BPNN model with different numbers of hidden layer nodes.

status of the preceding vehicle and the number of output nodes was confirmed as 1. The identification accuracy rates of the BPNN model with the number of hidden layer nodes ranging from 5 to 30 were calculated. The results are shown in Fig. 11. The peak value of the recognition accuracy rate was 84% for 6, 11, and 21 hidden layer nodes, indicating that the learning ability of the BPNN model for identifying the lane change status of the leading vehicle the same for different numbers of hidden layer nodes. However, the learning speeds were slower when the number of hidden layer nodes was 11 and 21 because of discrepancies caused by the complexity of the model structure. Therefore, we used a BPNN with 6 hidden layer nodes after comprehensive consideration of the learning speed and learning ability.

B. BPNN MODEL

In this study, a fixed time window with an optimal length was used to segment the data to improve the recognition accuracy and recognition efficiency of the proposed identification model. The lane change status of the leading vehicles had to be discerned before the leading vehicle crossed the lane for the following reasons. First, abundant traffic conflicts occur after vehicles cross lanes. Identifying the lane change status before the vehicles cross the lanes provides a warning to eliminate conflicts. Second, if the leading vehicle's distance to the lane was equal to 0, it indicated that the leading vehicle has crossed the lane. Therefore, discerning the lane change status after vehicles have crossed the lanes using the identification model is insignificant. In summary, the time window ought to be less than the average time required for vehicles to cross the lanes.

Based on 1170 lane change events, it was determined that the average time required for a lane change was 7.85 s and the average time required for a lane crossing was 2.01 s. Thus, the upper limit of the time window was determined to be 2.0 s. In order to improve the real-time performance of the identification model and the accuracy, the detection time should be as short as possible. In this study, the recognition rates of the BPNN model with different input parameters were calculated for time windows of 0.6, 0.8, 1.2, 1.4, 1.6, 1.8, and 2.0 s, respectively. The results are shown in Table 4 and Fig. 12. The results indicate that the identification model achieved

TABLE 4. Identification accuracy rate for different input parameters and different time windows.

Input parameter	0.6s	0.8s	1.0s	1.2s	1.4s	1.6s	1.8s	2.0s
LV	72%	71%	72%	76%	78%	79%	75%	81%
LD	71%	72%	71%	73%	73%	79%	79%	73%
LV, ZV	73%	71%	75%	79%	78%	80%	75%	83%
LD, ZV	74%	76%	76%	79%	77%	79%	73%	78%
LD, LV	75%	81%	80%	84%	84%	85%	83%	87%
LD,LV,ZV	80%	81%	81%	82%	84%	80%	84%	87%

TABLE 5. Percentage of lane crossing times longer than the disparate time windows.

Time window	Numbers	Percent (%)
0.6 s	219	100%
0.8 s	219	100%
1.0 s	215	98.2%
1.2 s	201	91.8%
1.4 s	192	87.7%
1.6 s	163	74.4%
1.8 s	143	65.3%
2.0 s	116	53%

high recognition accuracy rate when the combinations of input parameters were LD, LV, ZV and LD, LV. Considering the recognition efficiency, we wanted the fewest number of input parameters. Hence, LD and LV were determined as the ultimate combination of input parameters. In this case, the recognition accuracy of the neural network was higher than 85% when the time windows were 1.6 and 2.0 s.

The percentages of the lane crossing times of the leading vehicle that were longer than the disparate time windows relative to all lane change behaviors are shown in Table 5. The values indicate the suitability of the BPNN model. As shown in Table 5, as the time window increased, the percentage of lane crossing times with TLC longer than the time window decreased. The BPNN only can predicted 74.4% of the lane crossing times of the leading vehicles when the time window was 1.6 s. Therefore, if only the BPNN is used, the accuracy requirements of the recognition rate and recognition range are not met.

C. PSO-BPNN MODEL

In this study, the PSO algorithm was used to optimize the initial connection weights and thresholds of the BPNN model. The values of the acceleration coefficients c_1 and c_2 were 3 and 1, respectively. The maximum number of iterations was set to 300 and the predetermined fitness value ranged from 0.005 to 0.015. The PSO-BPNN structure was set as 4-6-1. Namely, the input layer had 4 nodes, the hidden layer had 6 nodes, and the output layer had 1 node. Therefore, the vector dimension of the particles was 37, as defined in (9). The neural network mapping was improved and the recognition rate of the BPNN model was optimized by the PSO for different input parameters and time windows of 0.6, 0.8, 1.2, 1.4, 1.6, 1.8, and 2.0 s. The results are shown in Table 6 and Fig. 13.

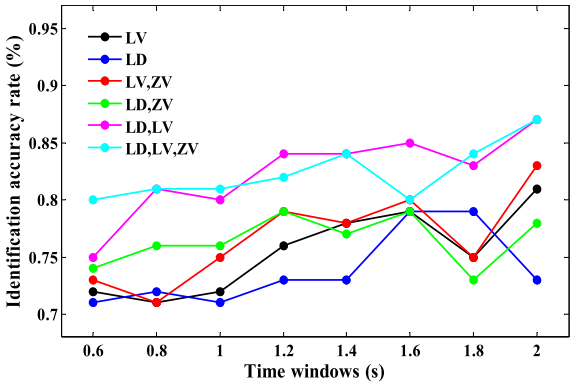

FIGURE 12. Identification accuracy rate for different input parameters and different time windows.

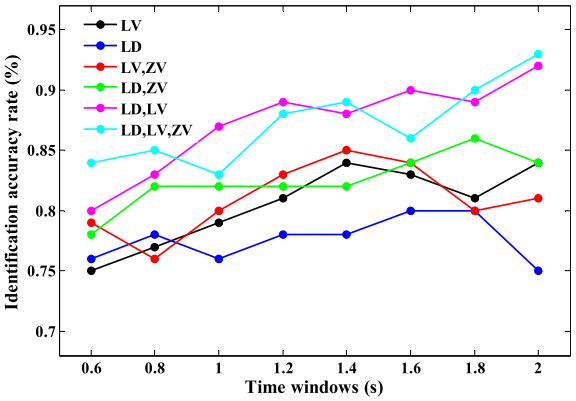

FIGURE 13. Identification accuracy rate for different input parameters and different time windows.

TABLE 6. Identification accuracy rate for different input parameters and different time windows.

Input parameter	0.6s	0.8s	1.0s	1.2s	1.4s	1.6s	1.8s	2.0s
LV	75%	77%	79%	81%	84%	83%	81%	84%
LD	76%	78%	76%	78%	78%	80%	80%	75%
LV, ZV	79%	76%	80%	83%	85%	84%	80%	81%
LD, ZV	78%	82%	82%	82%	82%	84%	86%	84%
LD, LV	80%	83%	87%	89%	88%	90%	89%	92%
LD,LV,ZV	84%	85%	83%	88%	89%	86%	90%	93%

The results in Table 4 and Table 6 indicate that the recognition accuracy rate of the lane change status of the leading vehicle by the BPNN model increased significantly after optimization with the PSO algorithm. The identification accuracy rate increased from 80% to 87% for the time window of 1.0 s and the same input parameters. The highest recognition accuracy rate was 93% for the 2.0 s time window and the combinations of input parameters of LD, LV, and ZV. However, the more rapidly the model detected the motion status of the preceding vehicle, the faster the other intelligent algorithm adjusted the motion status of the host vehicle. As shown in Fig. 13, the recognition accuracy rate improved as the time window increased beyond 1.0 s. After 1.0 s, the rate of increase of the recognition accuracy was lower

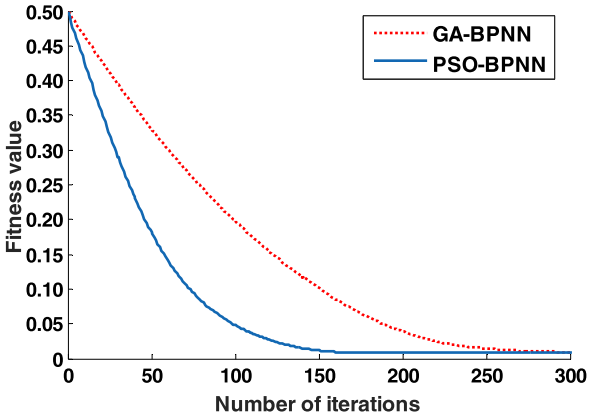

FIGURE 14. Comparison of the fitness values of two types of BPNN models.

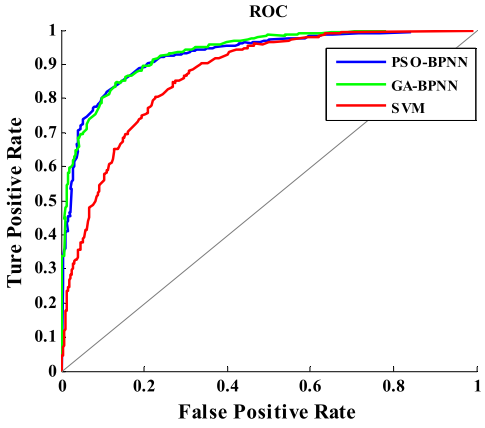

FIGURE 15. ROC curve.

than the rate of decrease of the application degree with the increase in the time window (i.e., Table 5). Although the recognition accuracy rate still remained high for the time windows of 1.2, 1.4, 1.6, 1.8, and 2.0 s, the application range of the proposed model became increasingly narrow as the time window increased. By synthetically considering the relationships among promptness, validity, and application range, we determined that 1.0 s was the optimum time window. As shown in Table 5, 98.2% of the lane crossing times of the leading vehicle could be predicted by the neural network model for the time window of 1.0 s and the recognition accuracy was 87%, indicating that the accuracy requirements were met.

The training results by comparison with the GA-BPNN is shown in Fig. 14. The fitness value were 0.011 and 0.126 respectively for 140 iterations. The results indicated that the PSO-BPNN reached the predetermined fitness value before the GA-BPNN. The fitness value of the GA-BPNN reached 0.015 at 250 iterations. The results demonstrated that the PSO-BPNN not only resulted in higher accuracy but also required less training time.

The receiver operating characteristic (ROC) curve was plotted to evaluate the recognition performance of the PSO-BPNN model because the recognition accuracy rate does not provide information on the errors associated with the lane changes. The ROC curve is an indicator of the detection sensitivity and specificity of the recognition model. In the ROC curve, the true positive (TP) represents the number of correctly identified lane changes among all lane change samples. The true negative (TN) represents the number of correctly identified no lane changes among all no lane change samples. The false positive (FP) represents the number of incorrectly identified no lane changes among all lane change samples. The false negative (FN) represents the number incorrectly identified lane changes among all no lane change samples. The recognition accuracy of the lane changes and no lane changes are referred to as sensitivity ($sen = \frac{TP}{TP+FN}$) and specificity ($spe = \frac{TN}{TN+FP}$), respectively. The horizontal and vertical coordinates of the ROC curve represent the calculated values of sensitivity and specificity, respectively. In general, the closer the value is to the upper left corner, the better the performance of the model is. The model performance was determined by the area under the ROC curve (AUC). A large AUC indicates a high identification accuracy of the model. In this study, the performances of the PSO-BPNN, GA-BPNN, and SVM were evaluated using the ROC curve. As shown in Fig. 15, the AUC was largest for the PSO-BPNN (0.9328), followed by the GA-BPNN (0.9311) and the SVM (0.8640). These results indicated that the proposed PSO-BPNN model had the best recognition accuracy.

D. CONTINUOUS IDENTIFICATION MODEL OF TLC

The PSO-BPNN model did not detect the lane change status of the leading vehicle when the time window was longer than the TLC. Statistics have shown that 1.8% of the lane changes of the leading vehicle were not identified before the lane crossing occurred when using a conventional classification model. The continuous recognition model of the TLC was used to address the drawbacks of the neural network model. The stationary time window was divided into five temporal intervals: (0 s, 0.2 s), (0.2 s, 0.4 s), (0.4 s, 0.6 s), (0.6 s, 0.8 s), and (0.8 s, 1.0 s). The frequency distribution of the TLC in each interval was determined statistically. Then, the lane change probability of each interval was calculated. The results are shown in Table 7 and indicate that the probability of the lane changes of the leading vehicle was generally lower than 75%. This result was not sufficient to determine the status using one TLC value. Each time the TLC value was transformed, the kinestate of the leading vehicle might change between lane change and no lane change. The frequency distribution of the TLC with a continuously decreasing trend in each interval was determined statistically. The results are shown in Table 8. The results indicated that the probability of lane changes of the leading vehicle continued to increase with the decrease in the time interval after the continuous recognition of TLC. The probability exceeded 88% in the time periods (0.4 s, 0.6 s), (0.2 s, 0.4 s), and (0 s, 0.2 s). However, the probability for the time periods (0.8 s, 1.0 s) and (0.6 s, 0.8 s) was still too low to identify lane changes. The continuous recognition model of TLC was

TABLE 7. Percentage of lane changes with first statistics.

Temporal interval	(0.8,1.0s)	(0.6,0.8s)	(0.4,0.6s)	(0.2,0.4s)	(0,0.2s)
Lane change	49%	51%	54%	57%	73%

TABLE 8. Percentage of lane changes with second statistics.

Temporal interval	(0.8,1.0s)	(0.6,0.8s)	(0.4,0.6s)	(0.2,0.4s)	(0,0.2s)
Lane change	74%	82%	88%	89%	91%

TABLE 9. Percentage of lane changes with third statistics.

Temporal interval	(0.8 s, 1.0s)	(0.6 s, 0.8s)
Lane change	88%	91%

used again for the low probability intervals. The distribution is shown in Table 9. The results indicated that the probability of lane changes of the leading vehicle continued to improve with the decrease in the time interval after three consecutive evaluations of the TLC. The probability for the time periods (0.8 s, 1.0 s) and (0.6 s, 0.8 s) surpassed 88% and thus this method was suitable to detect the lane changes.

In summary, the continuous recognition model of the TLC was applied to identify the lane change status of the leading vehicle with a TLC of less than 1.0 s. An additional estimation of the TLC was performed in the time periods (0.4 s, 0.6 s), (0.2 s, 0.4 s), and (0 s, 0.2 s). The lane change status was confirmed by the continuous decline in TLC. In time periods (0.8 s, 1.0 s) and (0.6 s, 0.8 s), two additional assessments of TLC were executed and the lane change status was determined by the continuous decline of the TLC. The recognition accuracy of this process for determining the lane change status of the leading vehicle was higher than 88% for the TLC of less than 1.0 s. By using the proposed models, almost all of the lane changes of the leading vehicles were detected before the vehicles crossed the lane.

VI. CONCLUSIONS

The recognition of lane change status of a distant leading vehicle is significant to improve the cognitive competence of autonomous driving systems. In this study, a comprehensive identification model for determining the lane change status of a leading vehicle was established by analyzing the lateral distance and lateral velocity of the leading vehicles using millimeter-wave radar data obtained in a naturalistic driving test. Due to the differences in TLC, the comprehensive identification model comprises a PSO-BPNN model and a continuous identification model for the TLC. Based on 1170 groups of lane change events recorded during the naturalistic on-road experiment, it was determined that 98.2% of the lane crossing times of the leading vehicle was longer than 1.0 s. Only 1.8% of the lane changes of the leading vehicle were not detected by the BPNN model when the time window was 1.0 s. The simulation results indicated that the recognition accuracy rate of the BPNN model increased from 80% to 87% after PSO optimization at TLCs longer than 1.0 s. Therefore, by considering the relationships among promptness, validity, and application range, we used 1.0 s as the optimal time window. The continuous recognition model of the TLC was used to address the drawbacks of the PSO-BPNN. When the TLC was shorter than 1.0 s, the recognition accuracy of the proposed model for the lane changes of the leading vehicle was higher than 88% due to the use of the continuous TLC model. The results of this study indicate that the implementation of the proposed comprehensive identification model for detecting the lane change status of leading vehicles significantly increased the identification accuracy, thereby providing a basis for improving the performance of intelligent perception systems. At present, the proposed model is only suitable for conventional lane change identification on straight lanes or curve lanes of expressways. A future study will consider complex lane change behaviors and different driving styles to enhance the fault tolerance of the proposed identification model.

REFERENCES

[1] P. Falcone, F. Borrelli, J. Asgari, H. E. Tseng, and D. Hrovat, "Predictive active steering control for autonomous vehicle systems," *IEEE Trans. Control Syst. Technol.*, vol. 15, no. 3, pp. 566–580, May 2007.
[2] P. Koopman and M. Wagner, "Autonomous vehicle safety: An interdisciplinary challenge," *IEEE Intell. Transp. Syst. Mag.*, vol. 9, no. 1, pp. 90–96, Jul. 2017.
[3] S. E. Shladover, "Cooperative (rather than autonomous) vehicle-highway automation systems," *IEEE Intell. Transp. Syst. Mag.*, vol. 1, no. 1, pp. 10–19, Jul. 2009.
[4] C. Hatipoglu, U. Ozguner, and K. A. Redmill, "Automated lane change controller design," *IEEE Trans. Intell. Transp. Syst.*, vol. 4, no. 1, pp. 13–22, Mar. 2003.
[5] Y. Guo, Q. Sun, R. Fu, and C. Wang, "Improved car-following strategy based on merging behavior prediction of adjacent vehicle from naturalistic driving data," *IEEE Access*, vol. 7, pp. 44258–44268, 2019.
[6] P. Koopman and M. Wagner, "Challenges in autonomous vehicle testing and validation," *SAE Int. J. Transp. Saf.*, vol. 4, no. 1, pp. 15–24, Apr. 2016.
[7] T. Mercy, R. Van Parys, and G. Pipeleers, "Spline-based motion planning for autonomous guided vehicles in a dynamic environment," *IEEE Trans. Control. Syst. Technol.*, vol. 26, no. 6, pp. 2182–2189, Nov. 2018.
[8] V. Subramanian, T. F. Burks, and A. A. Arroyo, "Development of machine vision and laser radar based autonomous vehicle guidance systems for citrus grove navigation," *Comput. Electron. Agricult.*, vol. 53, no. 2, pp. 130–143, 2006.
[9] Z. Gao, D. Y. Wang, S. H. Wan, H. Zhang, and Y. L. Wang, "Cognitive-inspired class-statistic matching with triple-constrain for camera free 3D object retrieval," *Future Gener. Comput. Syst.*, vol. 94, pp. 641–653, May 2019.
[10] A. Shaukat, P. C. Blacker, C. Spiteri, and Y. Gao, "Towards camera-LIDAR fusion-based terrain modelling for planetary surfaces: Review and analysis," *Sensors*, vol. 16, no. 11, p. 1952, 2016.
[11] S. Wan, Y. Zhao, T. Wang, Z. Gu, Q. H. Abbasi, and K.-K. R. Choo, "Multi-dimensional data indexing and range query processing via Voronoi diagram for Internet of Things," *Future Gener. Comput. Syst.*, vol. 91, pp. 382–391, Feb. 2019.
[12] M. Amoozadeh, A. Raghuramu, C.-N. Chuah, D. Ghosal, H. M. Zhang, J. Rowe, and K. Levitt, "Security vulnerabilities of connected vehicle streams and their impact on cooperative driving," *IEEE Commum. Mag.*, vol. 53, no. 6, pp. 126–132, Jun. 2015.
[13] R.-H. Zhang, Z.-C. He, H.-W. Wang, F. You, and K.-N. Li, "Study on self-tuning tyre friction control for developing main-servo loop integrated chassis control system," *IEEE Access*, vol. 5, pp. 6649–6660, 2017.

[14] S. J. Anderson, S. B. Karumanchi, and K. Iagnemma, "Constraint-based planning and control for safe, semi-autonomous operation of vehicles," in *Proc. IEEE Intell. Vehicles Symp.*, Jun. 2012, pp. 383–388.

[15] S. Ossen and S. Hoogendoorn, "Driver heterogeneity in car following and its impact on modeling traffic dynamics," *Transp. Res. Rec., J. Transp. Res. Board*, vol. 1999, no. 1, pp. 95–103, 2007.

[16] J. D. Alonso, E. R. Vidal, A. Rotter, and M. Muhlenberg, "Lane-change decision aid system based on motion-driven vehicle tracking," *IEEE Trans. Veh. Technol.*, vol. 57, no. 5, pp. 2736–2746, Sep. 2008.

[17] Y. He, D. Sun, M. Zhao, and S. Cheng, "Cooperative driving and lane changing modeling for connected vehicles in the vicinity of traffic signals: A cyber-physical perspective," *IEEE Access*, vol. 6, pp. 13891–13897, 2018.

[18] Y.-X. Huang, R. Jiang, H. M. Zhang, M.-B. Hu, J.-F. Tian, B. Jia, and Z.-Y. Gao, "Experimental study and modeling of car-following behavior under high speed situation," *Transp. Res. C, Emerg. Technol.*, vol. 97, pp. 194–215, Dec. 2018.

[19] R. Dang, J. Wang, S. E. Li, and K. Li, "Coordinated adaptive cruise control system with lane-change assistance," *IEEE Trans. Intell. Transp. Syst.*, vol. 16, no. 5, pp. 2373–2383, Oct. 2015.

[20] A. Pande and M. Abdel-Aty, "Assessment of freeway traffic parameters leading to lane-change related collisions," *Accident Anal. Prevention*, vol. 38, no. 5, pp. 936–948, 2006.

[21] J. Zheng, K. Suzuki, and M. Fujita, "Predicting driver's lane-changing decisions using a neural network model," *Simul. Model. Pract. Theory*, vol. 42, pp. 73–83, Mar. 2014.

[22] C. G. Prevost, A. Desbiens, and E. Gagnon, "Extended Kalman filter for state estimation and trajectory prediction of a moving object detected by an unmanned aerial vehicle," in *Proc. Amer. Control Conf.*, Jul. 2007, pp. 1805–1810.

[23] C. Hermes, C. Wohler, K. Schenk, F. Kummert, "Long-term vehicle motion prediction," in *Proc. IEEE Intell. Vehicles Symp.*, Jun. 2009, pp. 652–657.

[24] Y. Dou, F. Yan, and D. Feng, "Lane changing prediction at highway lane drops using support vector machine and artificial neural network classifiers," in *Proc. IEEE Int. Conf. Adv. Intell. Mechatron. (AIM)*, Jul. 2016, pp. 901–906.

[25] H. Hou, L. Jin, Q. Niu, Y. Sun, and M. Lu, "Driver intention recognition method using continuous hidden Markov model," *Int. J. Comput. Intell. Syst.*, vol. 4, no. 3, pp. 386–393, May 2011.

[26] Y. Li, Y. Ruichek, and C. Cappelle, "Optimal extrinsic calibration between a stereoscopic system and a LIDAR," *IEEE Trans. Instrum. Meas.*, vol. 62, no. 8, pp. 2258–2269, Aug. 2013.

[27] Z. Gao, H.-Z. Xuan, Z. Zhang, S. Wan, and K.-K. R. Choo, "Adaptive fusion and category-level dictionary learning model for multi-view human action recognition," *IEEE Internet Things J.*, to be published.

[28] H. Cheng, N. Zheng, X. Zhang, J. Qin, and H. Van De Wetering, "Interactive road situation analysis for driver assistance and safety warning systems: Framework and algorithms," *IEEE Trans. Intell. Transp. Syst.*, vol. 8, no. 1, pp. 157–167, Mar. 2007.

[29] S. Ding, S. Qu, Y. Xi, A. K. Sangaia, and S. Wan, "Image caption generation with high-level image features," *Pattern Recognit. Lett.*, vol. 123, pp. 89–95, May 2019.

[30] J. Peng, Y. Guo, R. Fu, W. Yuan, and C. Wang, "Multi-parameter prediction of drivers' lane-changing behaviour with neural network model," *Appl. Ergonom.*, vol. 50, pp. 207–217, Sep. 2015.

[31] A. Doshi and M. M. Trivedi, "On the roles of eye gaze and head dynamics in predicting driver's intent to change lanes," *IEEE Trans. Intell. Transp. Syst.*, vol. 10, no. 3, pp. 453–462, Sep. 2009.

[32] F. Lethaus and J. Rataj, "Do eye movements reflect driving manoeuvres?" *IET Intell. Transp. Syst.*, vol. 1, no. 3, pp. 199–204, Sep. 2007.

[33] L. Jin, H. Hou, and Y. Jiang, "Driver intention recognition based on continuous hidden Markov model," in *Proc. Int. Conf. Transp., Mech., Elect. Eng. (TMEE)*, Dec. 2011, pp. 742–793.

[34] C. Zong, C. Wang, D. Yang, and H. Yang, "Driving intention identification and maneuvering behavior prediction of drivers on cornering," in *Proc. Int. Conf. Mechatron. Automat.*, Aug. 2009, pp. 4055–4060.

[35] R. Zhao, W. Ouyang, and X. Wang, "Person re-identification by saliency learning," *IEEE Trans. Pattern Anal. Mach. Intell.*, vol. 39, no. 2, pp. 356–370, Feb. 2017.

[36] X. Guo, D. Dias, C. Carvajal, L. Peyras, and P. Breul, "Reliability analysis of embankment dam sliding stability using the sparse polynomial chaos expansion," *Eng. Struct.*, vol. 174, pp. 295–307, Nov. 2018.

[37] X. Xu, Y. Xue, L. Qi, Y. Yuan, X. Zhang, T. Umer, and S. Wan, "An edge computing-enabled computation offloading method with privacy preservation for Internet of connected vehicles," *Future Gener. Comput. Syst.*, vol. 96, pp. 89–100, Jul. 2019.

[38] S. Vogel, H. Ney, and C. Tillmann, "HMM-based word alignment in statistical translation," in *Proc. 16th Conf. Comput. Linguistics*, vol. 2, Aug. 1996, pp. 836–841.

[39] X. Sun, H. Zhang, W. Meng, R. Zhang, K. Li, and T. Peng, "Primary resonance analysis and vibration suppression for the harmonically excited nonlinear suspension system using a pair of symmetric viscoelastic buffers," *Nonlinear Dyn.*, vol. 94, no. 2, pp. 1243–1265, Oct. 2018.

[40] M. Gevrey, L. Dimopoulos, and S. Lek, "Review and comparison of methods to study the contribution of variables in artificial neural network models," *Ecol. Model.*, vol. 160, no. 3, pp. 249–264, Feb. 2003.

[41] M. Zhou, X. Qu, and X. Li, "A recurrent neural network based microscopic car following model to predict traffic oscillation," *Transp. Res. C, Emerg. Technol.*, vol. 84, pp. 245–264, Nov. 2017.

[42] M. Liu and J. Shi, "A cellular automata traffic flow model combined with a BP neural network based microscopic lane changing decision model," *J. Intell. Transp. Syst.*, vol. 23, no. 4, pp. 309–318, 2019.

[43] B. Aalizadeh and A. Asnafi, "Combination of particle swarm optimization algorithm and artificial neural network to propose an efficient controller for vehicle handling in uncertain road conditions," *Neural. Comput. Appl.*, vol. 30, no. 2, pp. 585–593, Jul. 2018.

[44] R. Geng, X. Wang, N. Ye, and J. Liu, "A fault prediction algorithm based on rough sets and back propagation neural network for vehicular networks," *IEEE Access*, vol. 6, pp. 74984–74992, 2018.

[45] S. Ding, C. Su, and J. Yu, "An optimizing BP neural network algorithm based on genetic algorithm," *Artif. Intell. Rev.*, vol. 36, no. 2, pp. 153–162, 2011.

[46] C. Ren, N. An, J. Wang, L. Li, B. Hu, and D. Shang, "Optimal parameters selection for BP neural network based on particle swarm optimization: A case study of wind speed forecasting," *Knowl. Based Syst.*, vol. 56, pp. 226–239, Jan. 2014.

[47] K. G. Kapanova, I. Dimov, and J. M. Sellier, "A genetic approach to automatic neural network architecture optimization," *Neural. Comput. Appl.*, vol. 29, no. 5, pp. 1481–1492, Mar. 2018.

[48] H. Taghavifar, A. Mardani, and A. H. Hosseinloo, "Appraisal of artificial neural network-genetic algorithm based model for prediction of the power provided by the agricultural tractors," *Energy*, vol. 93, pp. 1704–1710, Dec. 2015.

[49] B. Zhu, S. Yan, J. Zhao, and W. Den, "Personalized lane-change assistance system with driver behavior identification," *IEEE Trans. Veh. Technol.*, vol. 67, no. 11, pp. 10293–10306, Nov. 2018.

[50] H. Hao, Q. Zhang, Z. Wang, and J. Zhang, "Forecasting the number of end-of-life vehicles using a hybrid model based on grey model and artificial neural network," *J. Cleaner Prod.*, vol. 202, pp. 684–696, Nov. 2018.

[51] X. Liu, Y. Zhou, Z. Wang, and X. Chen, "A BP neural network-based communication blind signal detection method with cyber-physical-social systems," *IEEE Access*, vol. 6, pp. 43920–43935, 2018.

[52] W. Wei, G. Feng, Z. Li, and Y. Xu, "Deterministic convergence of an online gradient method for BP neural networks," *IEEE Trans. Neural Netw.*, vol. 16, no. 3, pp. 533–540, May 2005.

[53] S. Yu, K. Zhu, and F. Diao, "A dynamic all parameters adaptive BP neural networks model and its application on oil reservoir prediction," *Appl. Math. Comput.*, vol. 195, no. 1, pp. 66–75, 2008.

[54] W. Zheng, D.-H. Lee, and Q. Shi, "Short-term freeway traffic flow prediction: Bayesian combined neural network approach," *J. Transp. Eng.*, vol. 132, pp. 114–121, Sep. 2006.

[55] Z. Li, Q. Lei, X. Kouying, and Z. Xinyan, "A novel BP neural network model for traffic prediction of next generation network," in *Proc. 5th Int. Conf. Natural Comput.*, Aug. 2009, pp. 32–38.

[56] L. Wang, Y. Zeng, and T. Chen, "Back propagation neural network with adaptive differential evolution algorithm for time series forecasting," *Expert Syst. Appl.*, vol. 42, no. 2, pp. 855–863, 2015.

[57] J. Robinson and Y. Rahmat-Samii, "Particle swarm optimization in electromagnetics," *IEEE Trans. Antennas Propag.*, vol. 52, no. 2, pp. 397–407, Feb. 2004.

[58] J. R. Zhang, J. Zhang, T. M. Lok, and M. R. Lyu, "A hybrid particle swarm optimization–back-propagation algorithm for feedforward neural network training," *Appl. Math. Comput.*, vol. 185, no. 2, pp. 1026–1037, Feb. 2007.

[59] J. Upendar, C. P. Gupta, G. K. Singh, and G. Ramakrishna, "PSO and ANN-based fault classification for protective relaying," *IET Gener., Transmiss. Distrib.*, vol. 4, no. 10, pp. 1197–1212, Oct. 2010.

[60] B. Sinopoli, L. Schenato, M. Franceschetti, K. Poolla, M. I. Jordan, and S. S. Sastry, "Kalman filtering with intermittent observations," *IEEE Trans. Autom. Control.*, vol. 49, no. 9, pp. 1453–1464, Sep. 2004.
[61] H. Xiong, X. Zhu, and R. Zhang, "Energy recovery strategy numerical simulation for dual axle drive pure electric vehicle based on motor loss model and big data calculation," *Complexity*, vol. 2018, May 2018, Art. no. 4071743.
[62] R. Mehra, "On the identification of variances and adaptive Kalman filtering," *IEEE Trans. Autom. Control*, vol. AC-15, no. 2, pp. 175–184, Apr. 1970.
[63] R. Jensen and Q. Shen, "Semantics-preserving dimensionality reduction: Rough and fuzzy-rough-based approaches," *IEEE Trans. Knowl. Data Eng.*, vol. 16, no. 12, pp. 1457–1471, Dec. 2004.
[64] S. T. Roweis and L. K. Saul, "Nonlinear dimensionality reduction by locally linear embedding," *Science*, vol. 290, no. 5500, pp. 2323–2326, Dec. 2000.

CHANG WANG received the B.Tech., M.S., and Ph.D. degrees in transportation safety engineering from Chang'an University, Xi'an, China, in 2005, 2009, and 2012, respectively.

He is currently an Associate Professor with the Department of Transportation Safety Engineering, School of Automobile, Chang'an University. His research interests include traffic optimization, driving behavior, and vehicle active safety.

QINYU SUN received the B.Tech. and M.S. degrees in vehicle engineering from the Xi'an University of Science and Technology, Xi'an, China, in 2013 and 2016, respectively. He is currently pursuing the Ph.D. degree in vehicle engineering with the School of Automobile, Chang'an University. His research interests include autonomous driving, human–machine collaboration control, and vehicle active safety.

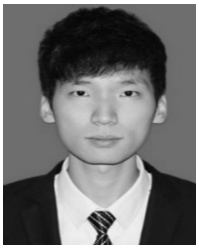

ZHEN LI received the B.S. degree in vehicle engineering from the Shandong University of Technology, Chengdu, China, in 2013, and the M.S. degree in vehicle engineering from Xihua University, Chengdu, in 2016. He is currently pursuing the Ph.D. degree in vehicle application engineering with the School of Automobile, Chang'an University. He was a Visiting Scholar with the University of Minnesota Twin Cities. His research interests include distraction driving, driving style, and car sickness.

HONGJIA ZHANG received the B.Tech. and M.S. degrees in transportation engineering from the Shandong University of Technology, Zibo, China, in 2014 and 2017, respectively. He is currently pursuing the Ph.D. degree in transportation engineering with the School of Automobile, Chang'an University. His research interests include autonomous driving, human–machine collaboration control, and vehicle active safety.

KAILI RUAN received the B.Tech. and M.S. degrees in transportation safety engineering and vehicle application engineering from Chang'an University, Xi'an, China, in 2015 and 2018, respectively. She is currently with the Technology Center, Shanghai Automotive Group Company Ltd. Her research interests include autonomous driving, ADAS systems, and vehicle active safety.